Korean J. Chem. Eng., **31**(9), 1532-1538 (2014)
DOI: 10.1007/s11814-014-0114-3

pISSN: 0256-1115
eISSN: 1975-7220

Semi-empirical modeling of carbonator with the physico-chemical characteristics of sorbent activity parameterized by the partial least squares method

Kee-Youn Yoo*, Dong-Yoon Shin, and Myung-June Park***,****,†**

*Department of Chemical and Biomolecular Engineering, Seoul National University of Science and Technology, Seoul 137-743, Korea
**Department of Energy Systems Research, Ajou University, Suwon 443-749, Korea
***Department of Chemical Engineering, Ajou University, Suwon 443-749, Korea
(*Received 26 February 2014 • accepted 16 April 2014*)

Abstract−We developed an evaluation module to calculate the carbon capture efficiency of a fluidized bed carbonator via the semi-empirical modeling of the solvent activity of lime particles. Since the solvent activity is affected by regeneration cycle number, reactor temperature, and particle size, two design parameters for the particle activity model, i.e., the characteristic time (t*) and the maximum conversion of particles (X_N), were determined as functions of the carbonator operating conditions by applying the partial least square (PLS) method to experimental data reported in the literature. The validity of the proposed approach was shown, and the effects of reactor design factors on the carbonator performance are discussed by means of appropriate simulation studies.

Keywords: Carbonator, Carbon Capture Efficiency, Semi-empirical Modeling, Partial Least Squares

INTRODUCTION

Carbon dioxide (CO_2) is one of the most significant anthropogenic emissions that contribute to recent changes in the global climate system [1,2], and growing concerns for global warming and climate change have motivated research activities toward developing more efficient and improved processes for CO_2 capture from its large point sources [3,4].

CO_2-capture processes are classified into pre-combustion, post-combustion, and oxyfuel-combustion, of which amine-based absorption systems for the post-combustion route are the only proven commercially available technology for current combustion systems [5]. However, this technology has several disadvantages, including its high-energy consumption for solvent regeneration, a high rate of process equipment corrosion, large solvent losses due to evaporation, and high solvent degradation rates in the presence of oxygen. These efficiency penalties and added costs justify the search for a range of emerging approaches that claim to be more energy efficient and cost effective than low-temperature absorption-based systems [5,6], and much research effort is being made in the development of an efficient dry absorbent-based fluidized-bed reactor with a looping cycle.

This type of looping cycle uses a very cheap and widely available recyclable sorbent that allows high makeup flows of fresh sorbent at a reasonable cost [7]; furthermore, these sorbents have high capacities for CO_2 chemisorption, lower heat capacities, and can produce pure CO_2 in regeneration cycles [6]. In addition, fluidization facilitates excellent heat transfer, uniform and controllable temperatures, favorable gas-solid contacting, and the ability to handle a wide variation in particulate properties [8].

There are several research works proposing a range of CaO-based solid looping systems for low cost and more energy efficient CO_2 capture technologies [9,10]. In CaO-based carbonators, CaO is carbonated to $CaCO_3$ at a relatively low temperature (*ca.* 600-700 °C) in flue gases at atmospheric pressure, while the calcination of $CaCO_3$ regenerates the sorbent to CaO and produces a concentrated stream of CO_2 at a higher temperature (>900 °C) [11, 12]. Cao et al. [5] simulated the local time-averaged CO_2 molar fraction and CaO conversion under a variety of operating conditions such as different cycle numbers, reaction temperatures, and mean particle sizes. Arias et al. [9] showed that the sorption capacity of a sorbent during cyclic testing depends on the experimental conditions if the sorbent is allowed to react under a slow diffusion-controlled regime.

In the area of reactor modeling, Kunii and Levenspiel [13] developed the K-L model to explain and correlate the observed rate data for physical and chemical phenomena occurring in fluidized beds with gas-solid mass transfer, gas-solid heat transfer, and solid catalyzed chemical reactions considered as factors. The model was extensively used to adopt reactivity data from laboratory tests of sorbent deactivation [14]. Meanwhile, there are several reports of simple and empirical reactor models to describe the apparent kinetics of CaO-carbonation [15,16].

We extended a semi-empirical model of dry particles, suggested by Alonso et al. [15] to implement a general-purpose economic evaluation module for dry sorbent-based fluidized bed reactors. The two main parameters should be determined to predict the activity of particles: the characteristic time (t*) and the maximum conversion of particles (X_N). Although experimental data showed that both t* and X_N are influenced by operating conditions such as particle size, regeneration cycle number, and carbonator temperature, this feature has not been adequately considered in the literature [15]. Therefore, in the present study, both were assumed to be functions of operating

†To whom correspondence should be addressed.
E-mail: mjpark@ajou.ac.kr

conditions to capture their physic-chemical characteristics and improve the performance of the model; meanwhile, in the evaluation module, the correlation between these activity-related parameters and the corresponding operating conditions was determined using a partial least squares (PLS) method. Experimental data for the fluidized bed carbonator, available in the literature [5], were used to investigate the validity of the proposed approach.

MATHEMATICAL MODELING

1. Fluidized-bed Carbonator Reactor Model

The carbonation reaction has a fast kinetic-controlled regime followed by a slow CO_2 diffusion-controlled regime. However, the fast regime is particularly representative of commercial-scale processes. Alonso et al. [15] reported that, in the fast carbonation regime when the operation time (t) is lower than a characteristic time (t*), the reaction has a reasonable constant rate, and the reaction extinguishes after t*, as follows:

$$r_{CaO}=\begin{cases}\dfrac{X_N}{t^*} & \text{for } t<t^*\\ 0 & \text{for } t>t^*\end{cases} \tag{1}$$

In Eq. (1), X_N represents the maximum obtainable conversion of dry particles in the N cycle, and it usually decreases with increasing cycle number. Alonso et al. [15] assumed a constant value of t^*, whereas, in contrast, experimental observations of CaO conversion profiles show different values of t^* with varying operating conditions (see Table 1). Therefore, the values of t^* and X_N are correlated for each set of operating conditions, and then the partial least squares model is applied in order to eliminate the data measurement noise and error.

Alvarez and Abanades [17] established that for most limestone types and reaction cycle numbers, the conversion of sorbent particles reaches X_N when the reaction front is at a distance of *ca.* 50 nm from the pore wall. Thus, the specific reaction surface S_N and X_N at the beginning of the N cycle can be related to each other as follows:

$$X_N=\left(e_{max}S_N\frac{\rho_{CaCO_3}}{M_{CaCO_3}}\right)\Big/\left(\frac{\rho_{CaO}}{M_{CaO}}\right) \tag{2}$$

Assuming that kinetic control of CaO with CO_2 dominates during the fast reaction regime, the following rate expression is obtained:

$$r_{CO_2}=k_S S_N(C_{CO_2}-C_{CO_2,e}) \tag{3}$$

On the basis of the above assumption, the overall activity of the particles in a batch of the N^{th} carbonation cycle is determined as follows:

$$f_a=1-\frac{X}{X_N} \tag{4}$$

Eq. (4) calculates the fraction, f_a, of lime that reacts in the carbonator. With the PLS-correlated sorbent activity model and the assumptions of gas plug flow and perfect mixing of solids, the CO_2 mass balance in the gas phase of the carbonator reactor can be written as follows:

$$\begin{aligned}F_{CO_2,in}\frac{dE_{carb}}{dz}&=Af_a\frac{\rho_{CaO}}{M_{CaO}}r_{CO_2}\\&=Af_a\frac{\rho_{CaO}}{M_{CaO}}k_S S_N C_{in}\left[f_{in}\left(\frac{1-E_{carb}}{1-f_{in}E_{carb}}\right)-f_e\right]\end{aligned} \tag{5}$$

Here, E_{carb} and $F_{CO_2,in}$ represent the capture efficiency and feed flow

Table 1. Experimental conditions[a] and data

No.	Conditions			Data		Remark
	Cycle (N)	Temperature [K]	Average particle diameter [mm]	t* [sec]	X_N	
1	1	928	0.5	138.9	0.512	Cycle number
2	10	928	0.5	103.7	0.246	
3	50	928	0.5	90	0.115	
4	120	928	0.5	87.4	0.108	
5	35	973	0.5	69	0.12	Temperature
6	35	923	0.5	57	0.121	
7	35	873	0.5	75	0.11	
8	35	823	0.5	67	0.078	
9	140	973	0.5	51.8	0.074	
10	140	923	0.5	66	0.066	
11	140	873	0.5	78	0.067	
12	1	928	0.33	129.5	0.629	Particle size
13	1	928	0.5	164.2	0.614	
14	1	928	0.7	175.3	0.557	
15	1	928	0.9	189.5	0.486	
16	30	928	0.33	111	0.123	
17	30	928	0.5	105	0.144	
18	30	928	0.7	123	0.127	
19	30	928	0.9	129	0.131	

[a]Pressure=0.7 bar; gas composition (CO_2 : Air)=15 : 85

rate of CO_2 in the carbonator, respectively, and k_s, f_{in}, and C_{in} in the right-hand side of Eq. (5) denote the kinetic rate constant, molar fraction of CO_2, and the feed CO_2 concentration at the inlet of the carbonator reactor, respectively. The derivation of the balance equation is described in the literature [15].

2. Partial Least Squares Model

A general method for the construction of a model with the relationship Y=f(X) is multiple linear regression (MLR) [18]. This can be represented mathematically as:

$$\mathbf{Y}=\mathbf{XB}+\mathbf{E}_{MLR} \tag{6}$$

where **X**, **Y**, **B**, and $\mathbf{E}_{MLR}$ represent the regressor (or input) block, the response (or output) block, the regression (or sensitivity) matrix, and the residual matrix, respectively. When the number of independent variables (m) is lower than the number of samples (n), there is no exact solution, but an approximate solution can be determined by minimizing the magnitude of the residual vector ($\mathbf{E}_{MLR}$). The least squares solution is given by:

$$\mathbf{B}=(\mathbf{X}^T\mathbf{X})^{-1}\mathbf{X}^T\mathbf{Y} \tag{7}$$

This equation reveals a common problem in MLR, namely, that the inverse of $\mathbf{X}^T\mathbf{X}$ may be difficult to compute if the input data block is of a high dimension and its elements are highly correlated, and these are referred to as instances of collinearity or singularity. The PLS approach provides an alternative to overcome this problem.

PLS methods involve an approximation of the **X** and **Y** spaces with their respective score matrices and the maximization of the correlation between the original data blocks [18,19]. A simplified model consists of a regression between the scores for the **X** and **Y** blocks. The PLS model can be interpreted as consisting of outer relations (**X** and **Y** blocks individually) and an inner relation (linking both blocks). The outer relations for the **X** and **Y** blocks are:

$$\mathbf{X}=\mathbf{TP}^T+\mathbf{E}=\sum_{h=1}^{a}\mathbf{t}_h\mathbf{p}_h^T+\mathbf{E} \tag{8}$$

$$\mathbf{Y}=\mathbf{UQ}^T+\mathbf{F}^*=\sum_{h=1}^{a}\mathbf{u}_h\mathbf{q}_h^T+\mathbf{F}^* \tag{9}$$

Each pair of latent variables accounts for a certain amount of the variability in the input and output blocks. The first a latent variables account for most of the variance of the data blocks, and the other latent variables capture measurement and/or process noise in the data. Both latent variables describe **Y** accurately (make $\|\mathbf{F}^*\|$) and, at the same time, determine a representative relationship between **X** and **Y**. A simple criterion for model building is to use a threshold value for **F***, but cross-validation can be used to determine the number of latent variables for a robust model [20].

The simplest model for the inner relation is a linear one:

$$\hat{\mathbf{u}}_h=b_h\mathbf{t}_h \tag{10}$$

where $b_h=\hat{\mathbf{u}}_h\mathbf{t}_h/\mathbf{t}_h^T\mathbf{t}_h$ plays the role of the regression coefficient in the multiple linear regression (MLR) and the principal component regression (PCR) model. Finally, the prediction model for quality variables is constructed applying the PLS algorithm in linear regression form as follows [21-23]:

$$\hat{\mathbf{y}}_h=\mathbf{x}^T\hat{\mathbf{b}} \tag{11}$$

RESULTS AND DISCUSSION

1. Prediction of t* and X_N as Functions of Operating Conditions

To obtain the correlation equation of t* and X_N using the PLS method, the cycle number (N), temperature (T), and particle diameter (d_p) were specified as manipulated variables, and 19 experimental conditions were selected from the literature (*cf.* Table 1) [5]. In addition, non-linear terms were included in the input vector to address the nonlinearity of the relationship as follows:

$$\mathbf{x}^T=[x_i, x_i^2, x_ix_{j(\neq i)}, \ln x_i] \qquad \text{where } x_1=N;\ x_2=T;\ x_3=d_p \tag{12}$$

The values of t* and X_N were determined by applying a method in the literature [15], where particles with a residence time higher than t* are shown to reach their maximum average conversion, X_N, and their reaction rate is zero from that time onwards. By contrast, particles with a residence time lower than t* approach their maximum conversion at a reaction rate that is constant for a given cycle number.

Fig. 1 illustrates how these points were determined along the time evolution of CaO conversion under specified operating conditions. As the number of experimental conditions is 19, the input data block (**X**) is a 19×11 matrix, while the output data block (**Y**) contains two properties (t* and X_N) under the corresponding experimental conditions. The input and output data blocks are scaled to prevent an ill-conditioning problem resulting from different orders of magnitude between variables in such a way that all the variables have means and variances of 0 and 1, respectively.

As shown in Eqs. (8) and (9), and the corresponding discussion (*cf.* '2. Partial Least Squares Model' section), the input and output blocks are projected onto new space, and the number of the latent variables is one of the important design parameters to determine the variances of two blocks. Therefore, it is important to determine

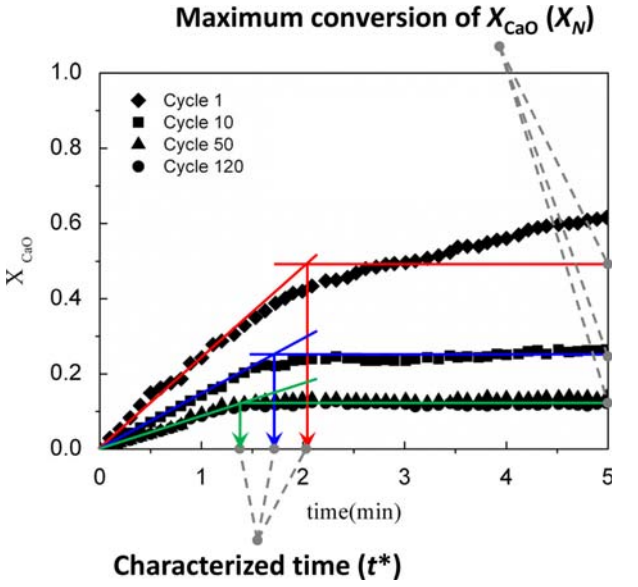

Fig. 1. Schematic diagram to determine the values of characteristic time (t*) and maximum X_{CaO} conversion (X_N) as functions of the cycle number. Experimental data are available in [5].

Table 2. PLS modeling coefficients for the prediction of t* and X_N[a]

Output \ Input	$\tilde{x}_1$	$\tilde{x}_2$	$\tilde{x}_3$	$\tilde{x}_1^2$	$\tilde{x}_2^2$	$\tilde{x}_3^2$	$\tilde{x}_1\tilde{x}_2$	$\tilde{x}_2\tilde{x}_3$	$\ln\tilde{x}_1$	$\ln\tilde{x}_2$	$\ln\tilde{x}_3$
$\tilde{y}_1$	−6.68e-2	8.64e-3	9.16e-2	0.19	−6.41e-3	0.12	−7.70e-2	9.13e-2	−0.79	2.34e-2	4.37e-2
$\tilde{y}_2$	−3.68e-2	1.58e-2	−1.49e-2	0.34	−4.47e-3	2.76e-2	−5.08e-2	−1.28e-2	−1.11	3.58e-2	−7.74e-2

[a]Subscript i of x_i: 1=cycle number, 2=temperature, 3=particle diameter; subscript i of y_i: 1=t*, 2=X_N. Variables x_i and y_i were scaled as $\tilde{x}_i = (x_i - m_i)/\sigma_i$, where m_i and σ_i represent the mean and the standard deviation of the data, respectively

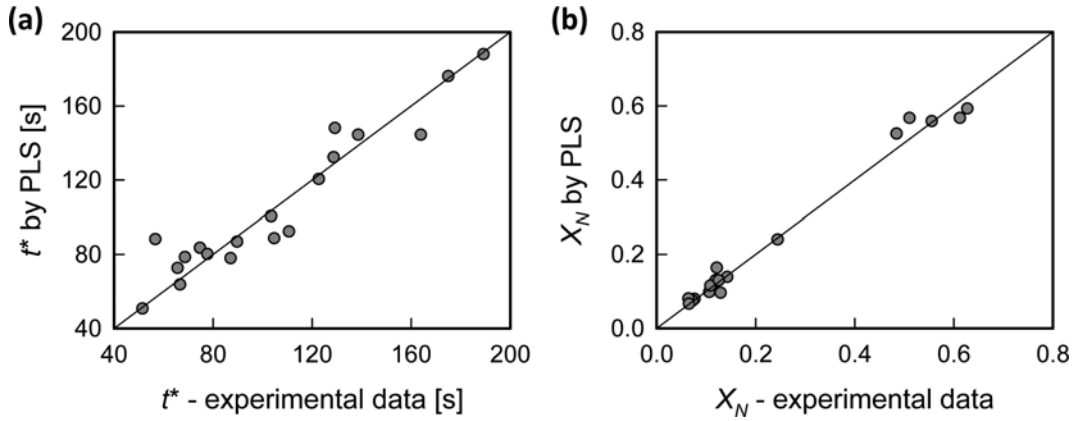

Fig. 2. Parity plots of (a) characteristic time (t*) and (b) maximum CaO conversion (X_N) between experimental data and simulated results obtained using the partial least squares (PLS) method. The means of the absolute relative residuals (MARR) and relative standard deviation of errors (RSDE) are (a) 9.1% and 8.5%, respectively, and (b) 8.0% and 9.4%, respectively.

this number adequately. PLS modeling shows that the first four latent variables cover more than 99% and 91% variances of the input and output blocks, respectively, while the other latent variables capture *ca*. 10% of the output data block, which may describe not only the noise in the data but also the errors that occur when determining the values from experimental data in the figures. Therefore, only four latent variables are used, and the resulting values are provided in Table 2. Fig. 2 shows the comparison between the experimental data and the simulation results, and it is clear that the performance of the PLS-based model is satisfactory.

The simulation results in Fig. 3 clearly show the effects of cycle number, reaction temperature, and particle size on both t* and X_N. In particular, there exists an unavoidable decrease in sorbent activity (X_N) that depends almost exclusively on the number of carbonation/calcination cycles and, to a lesser extent, on the reaction conditions. It is well known that the sintering of CaO during calcination causes a sharp reduction in surface area and a decline in X_N with N [24]. In addition, the carbonation rate (X_N/t*) also decreases with increasing N and as the mean sorbent particle size increased (graph not shown), but the extent of the rate decrease with increasing N was more significant than the effect of the mean particle size.

2. Kinetic Parameter Estimation

To estimate the kinetic parameters (k_S in Eq. (5)), CaO conversions were measured every 0.5 min over 3 min for each experimental condition (*cf.* Table 1). The kinetic parameters were fitted to the experimental data by minimizing the following objective function:

$$F_{obj} = \sum_{p}^{N_{exp}} \left[\sum_{q}^{NE} w_q \left(\frac{X_{q,calc} - X_{q,exp}}{X_{q,exp}} \right)^2 \right]_p \quad (13)$$

where X represents the CaO conversion, which was calculated by integrating the carbonation efficiency (E_{carb}) over time. In other words, Eq. (5) was solved every second, and the cumulative values of E_{carb} were obtained by mensuration-by-parts. Then, those values were algebraically manipulated using the inlet molar flow rate of CO_2 and molecular weights of each species to calculate the time profile of the CaO conversion. The subscripts "exp" and "calc" denote the experimental data and simulated results, respectively.

The estimation was conducted for each experimental run by using the *lsqcurvefit* function in MATLAB (MathWorks, Inc.), which applies the Levenberg-Marquardt algorithm for the optimization. The means of absolute relative residuals (MARR), defined as $100\sum|(y_{calc} - y_{exp})/y_{exp}|/N_{exp}$, and the corresponding relative standard deviations of the individual errors are 10.0 and 4.2%, respectively. Fig. 4 compares the calculated CaO conversion with that in the experimental data (total matrix of 19×6=114 elements), and also compares the simulation results with the estimated parameters.

To calculate the temperature dependency of the kinetic parameters, the estimated values at different temperatures were fitted to an Arrhenius type equation, and the result is provided in Fig. 5. The resulting equation is ln k=(−11.55)−8709/T or, equivalently, $k = 9.64\times10^{-6}\exp(-8709/T)$ where T is in K. The corresponding activation energy is 72 kJ/mol. The estimated parameters in the present study ranged between 3.9×10^{-10} and 1.4×10^{-9}, while reported values were 3.2×10^{-10}–8.9×10^{-10}, indicating that the estimated kinetic parameters are reasonable in comparison with those in literature data [7,14,17].

3. Effects of Operating Conditions

The reactor evaluation module with the PLS-correlated sorbent activity model was applied to operating conditions representative of a real case (a power plant delivering a given flow rate of CO_2, F_{CO_2}). As in the case of any fluidized bed reactor, there is a need for

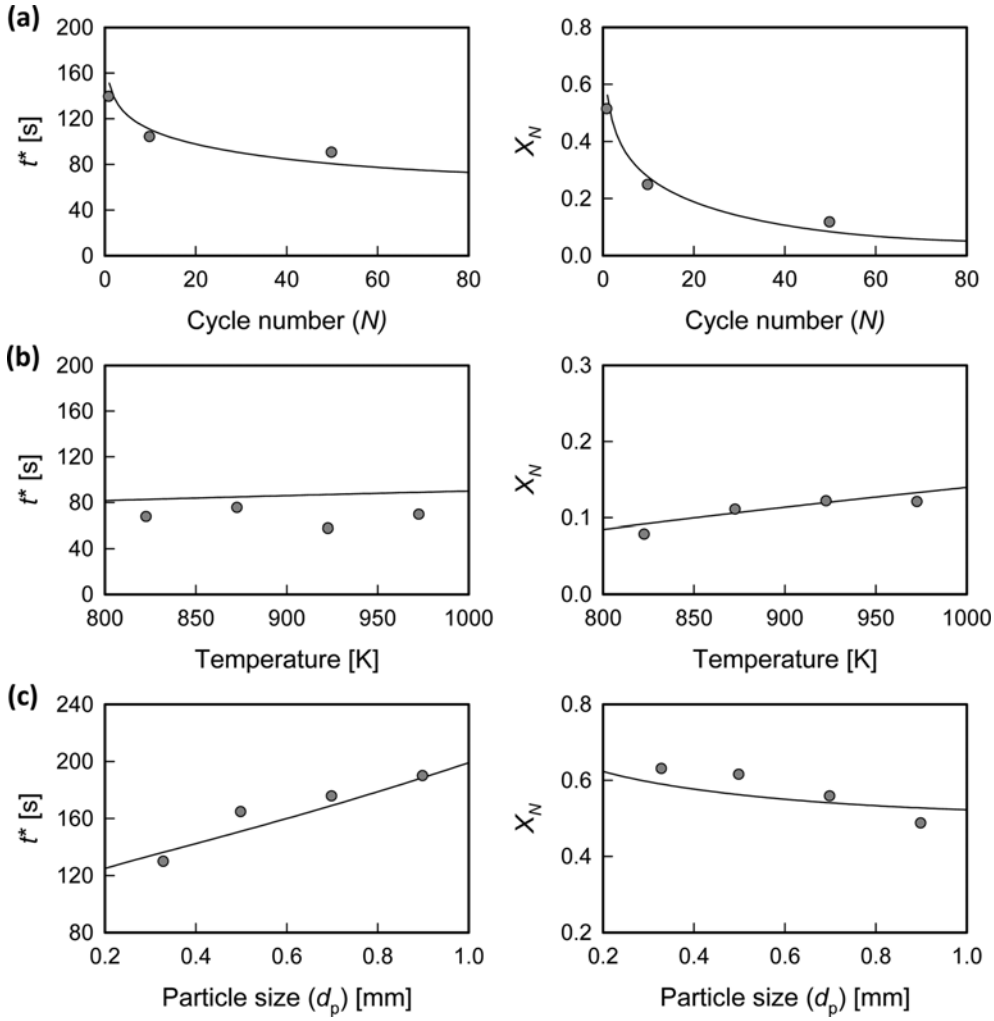

Fig. 3. Effects of (a) cycle number (T=928 K, d_p=0.5 mm), (b) temperature (N=35, d_p=0.5 mm), and (c) particle size (N=1, T=928 K) on the characteristic time (t*) [left] and maximum CaO conversion (X_N) [right].

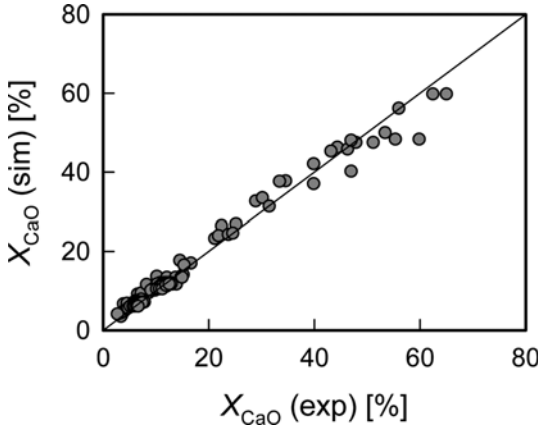

Fig. 4. Parity plots of CaO conversion (X_{CaO}) between experimental data and simulated results. MARR and RSDE are 10.0% and 4.2%, respectively.

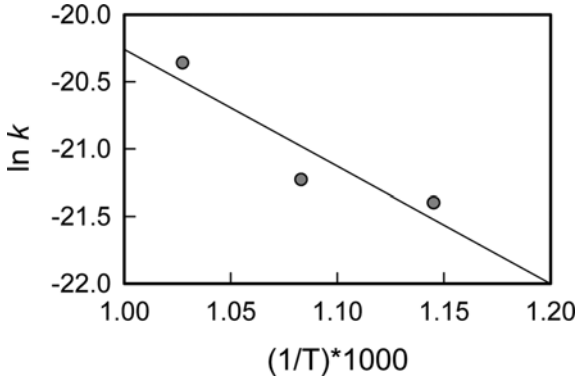

Fig. 5. Arrhenius fitting of kinetic constant, where ln k=(–11.55)–8709/T with r^2=0.8462.

a good knowledge of the fluid dynamics of the fluidized bed carbonator to determine the solid content (W_{CaO}) and the gas-solid contact quality. However, it is beyond the scope of the present work to incorporate a fluid dynamic sub-model into the carbonator evaluation module. Instead, the objective of the module is to achieve a reasonable estimate of the carbon capture efficiency to determine the economics of the reactor. The module described in the previous sections is able to calculate this efficiency when t*, X_N, and k_s can be estimated from laboratory experiments.

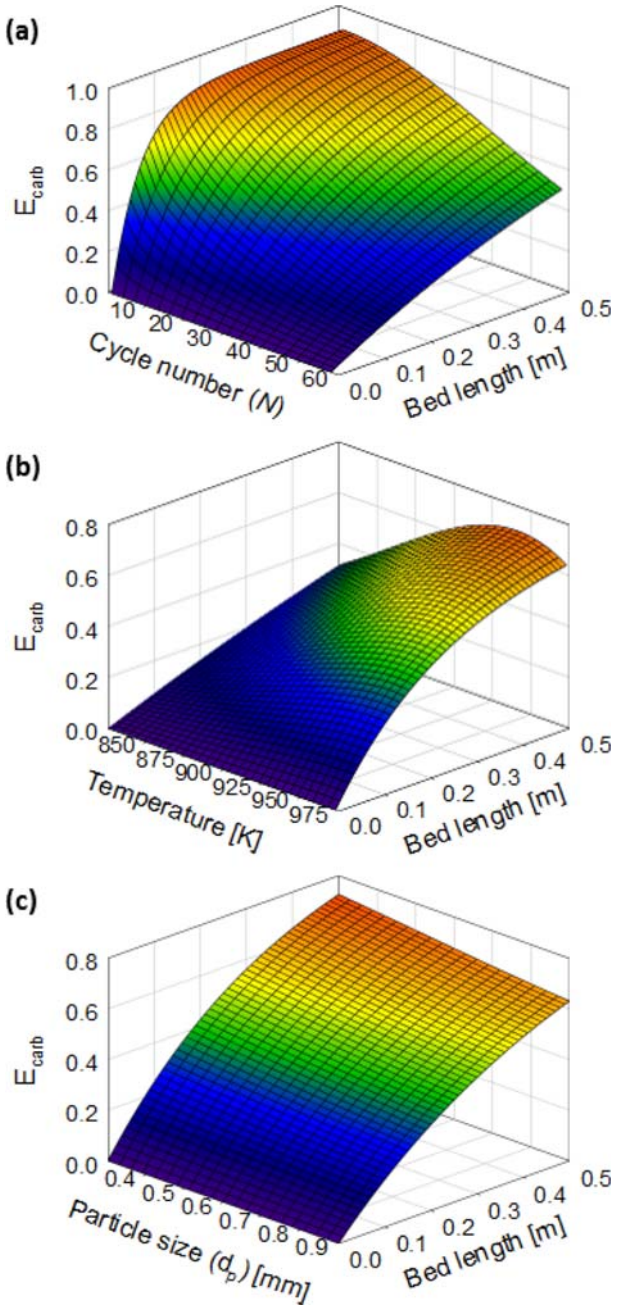

Fig. 6. Effects of (a) cycle number (T=928 K, d_p=0.5 mm), (b) temperature (N=35, d_p=0.5 mm), and (c) particle size (N=35, T=928 K) on the profile of the carbonation efficiency (E_{carb}) along the bed length at 30 s.

Fig. 6 shows the response of carbon capture efficiency with respect to various reactor design factors: sorbent cycle number, carbonator temperature, and particle size. Fig. 6(a) shows that the optimum average cycle number needs to be determined for a reasonable bed length for the case of continuous operation. Fig. 6(b) shows that the maximum capture efficiency is obtained at a certain operating temperature. Note that the linear velocity was proportional to temperature when ideal gas behavior was applied. Therefore, the feature in Fig. 6(b) is attributable to the fact that the reaction rate increases with temperature, while the increased temperature leads to an increase in linear velocity, resulting in a decrease in the residence time of the gas. Moreover, Fig. 6(c) shows that the smaller particle size is beneficial to the process under normal fluidization conditions.

CONCLUSIONS

The simulation results in this work show that, for reported CaO experimental data, the CO_2 capture efficiency for a carbonator evaluation module can be evaluated when it is applied to combustion flue gases. The module also calculates the optimum conditions for the capture of CO_2 from the flue gas; these conditions include an optimum solid inventory and sufficient sorbent activity. The proposed module is based on very simple assumptions about the fluid dynamics of the gas (plug flow) and solid (instant and perfect mixing), but it can also incorporate useful information about sorbent activity via a PLS-based correlation. Thus, the module presented in this work may serve as a convenient tool for designing and optimizing post-combustion carbonate looping systems.

ACKNOWLEDGEMENTS

This work was supported by the Energy Efficiency & Resources Core Technology Program of the Korea Institute of Energy Technology Evaluation and Planning (KETEP) financed by the Ministry of Trade, Industry & Energy (MOTIE), Republic of Korea (No. 20122010200071).

NOMENCLATURE

A : carbonator section [m^2]
C_{CO_2} : concentration of CO_2 [mol/m^3]
$C_{CO_2,e}$: equilibrium concentration of CO_2 [mol/m^3]
C_{in} : carbonator inlet concentration [mol/m^3]
E_{carb} : CO_2 capture efficiency in the carbonator
f_a : volumetric fraction of CaO that reacts in the fast rate regime
f_e : molar fraction of CO_2 at equilibrium in the reaction condition
f_{in} : inlet molar fraction of CO_2
$F_{CO_2,in}$: inlet molar flow rate of CO_2 [mol/s]
e_{max} : maximum thickness of the $CaCO_3$ layer on the sorbent particle pore, 50 nm
k_s : kinetic rate constant [$m^4/mol/s$]
M_{CaCO_3} : molecular weight of $CaCO_3$ [g/mol]
M_{CaO} : molecular weight of CaO [g/mol]
r_{CaO} : carbonation rate of the active sorbent [s^{-1}]
r_{CO_2} : consumption rate of CO_2 [s^{-1}]
S_N : reaction surface in the N cycle [m^{-1}]
t* : characteristic time at which the carbonation rate becomes zero [s]
X : conversion of sorbent particles in the carbonator
X_N : maximum conversion of sorbent particles in the N cycle

Greek Letters

ρ : density [g/m^3]

REFERENCES

1. M. B. Andrés, T. Boyd, J. R. Grace, C. Jim Lim, A. Gulamhusein,

B. Wan, H. Kurokawa and Y. Shirasaki, *Int. J. Hydrog. Energy*, **36**, 4038 (2011).
2. J. Blamey, E. J. Anthony, J. Wang and P. S. Fennell, *Prog. Energy Combust. Sci.*, **36**, 260 (2010).
3. Z. Deng, R. Xiao, B. Jin and Q. Song, *Int. J. Greenhouse Gas Control*, **3**, 368 (2009).
4. A. Samanta, A. Zhao, G. K. H. Shimizu, P. Sarkar and R. Gupta, *Ind. Eng. Chem. Res.*, **51**, 1438 (2012).
5. C. Cao, K. Zhang, C. He, Y. Zhao and Q. Guo, *Chem. Eng. Sci.*, **66**, 375 (2011).
6. M. Kianpour, M. A. Sobati and S. Shahhosseini, *Chem. Eng. Res. Des.*, **90**, 2041 (2012).
7. G. S. Grasa and J. C. Abanades, *Ind. Eng. Chem. Res.*, **45**, 8846 (2006).
8. D. A. Nemtsov and A. Zabaniotou, *Chem. Eng. J.*, **143**, 10 (2008).
9. B. Arias, J. C. Abanades and G. S. Grasa, *Chem. Eng. J.*, **167**, 255 (2011).
10. A. Charitos, C. Hawthorne, A. R. Bidwe, S. Sivalingam, A. Schuster, H. Spliethoff and G. Scheffknecht, *Int. J. Greenhouse Gas Control*, **4**, 776 (2010).
11. F. Fan, Z. S. Li and N. S. Cai, *Energy Fuels*, **23**, 207 (2009).
12. A. Lasheras, J. Ströhle, A. Galloy and B. Epple, *Int. J. Greenhouse Gas Control*, **5**, 686 (2011).
13. D. Kunii and O. Levenspiel, *Ind. Eng. Chem. Proc. Des. Dev.*, **7**, 481 (1968).
14. J. C. Abanades, E. J. Anthony, D. Y. Lu, C. Salvador and D. Alvarez, *AIChE J.*, **50**, 1614 (2004).
15. M. Alonso, N. Rodríguez, G. Grasa and J. C. Abanades, *Chem. Eng. Sci.*, **64**, 883 (2009).
16. D. K. Lee, *Chem. Eng. J.*, **100**, 71 (2004).
17. D. Alvarez and J. C. Abanades, *Ind. Eng. Chem. Res.*, **44**, 5608 (2005).
18. P. Geladi and B. R. Kowalski, *Anal. Chim. Acta*, **185**, 1 (1986).
19. M. A. Sharaf, D. L. Illman and B. R. Kowalski, *Chemometrics*, Wiley, New York (1986).
20. G. Baffi, E. B. Martin and A. J. Morris, *Comput. Chem. Eng.*, **23**, 395 (1999).
21. J. Choi, M.-J. Park, J. Kim, Y. Ko, S.-H. Lee and I. Baek, *Korean J. Chem. Eng.*, **30**, 1187 (2013).
22. M. Lee, M.-J. Park, W. Jeon, J.-W. Choi, Y.-W. Suh and D. Suh, *Korean J. Chem. Eng.*, **28**, 2142 (2011).
23. M.-J. Park, M. T. Dokucu and F. J. Doyle, *Ind. Eng. Chem. Res.*, **43**, 7227 (2004).
24. J. C. Abanades and D. Alvarez, *Energy Fuels*, **17**, 308 (2003).